

High responsivity tin gallium oxide Schottky ultraviolet photodetectors

Partha Mukhopadhyay, and Winston V. Schoenfeld

Citation: *Journal of Vacuum Science & Technology A* **38**, 013403 (2020); doi: 10.1116/1.5128911

View online: <https://doi.org/10.1116/1.5128911>

View Table of Contents: <https://avs.scitation.org/toc/jva/38/1>

Published by the *American Vacuum Society*

ARTICLES YOU MAY BE INTERESTED IN

Surface reaction mechanisms during atomic layer deposition of zirconium oxide using water, ethanol, and water-ethanol mixture as the oxygen sources

Journal of Vacuum Science & Technology A **38**, 012401 (2020); <https://doi.org/10.1116/1.5122994>

Temperature-dependence of Cl_2/Ar ICP-RIE of polar, semipolar, and nonpolar GaN and AlN following BCl_3/Ar breakthrough plasma

Journal of Vacuum Science & Technology A **38**, 013001 (2020); <https://doi.org/10.1116/1.5123787>

Perspective: Ga_2O_3 for ultra-high power rectifiers and MOSFETS

Journal of Applied Physics **124**, 220901 (2018); <https://doi.org/10.1063/1.5062841>

Solar blind Schottky photodiode based on an MOCVD-grown homoepitaxial $\beta\text{-Ga}_2\text{O}_3$ thin film

APL Materials **7**, 022527 (2019); <https://doi.org/10.1063/1.5064471>

Schottky barrier diode based on $\beta\text{-Ga}_2\text{O}_3$ (100) single crystal substrate and its temperature-dependent electrical characteristics

Applied Physics Letters **110**, 093503 (2017); <https://doi.org/10.1063/1.4977766>

A review of Ga_2O_3 materials, processing, and devices


Applied Physics Reviews **5**, 011301 (2018); <https://doi.org/10.1063/1.5006941>



Instruments for Advanced Science

Contact Hiden Analytical for further details:
W www.HidenAnalytical.com
E info@hiden.co.uk

CLICK TO VIEW our product catalogue




Gas Analysis

- dynamic measurement of reaction gas streams
- catalysis and thermal analysis
- molecular beam studies
- dissolved species probes
- fermentation, environmental and ecological studies




Surface Science

- UHV-TPD
- SIMS
- end point detection in ion beam etch
- elemental imaging - surface mapping



Plasma Diagnostics

- plasma source characterization
- etch and deposition process reaction kinetic studies
- analysis of neutral and radical species



Vacuum Analysis

- partial pressure measurement and control of process gases
- reactive sputter process control
- vacuum diagnostics
- vacuum coating process monitoring


High responsivity tin gallium oxide Schottky ultraviolet photodetectors

Cite as: J. Vac. Sci. Technol. A 38, 013403 (2020); doi: 10.1116/1.5128911

Submitted: 24 September 2019 · Accepted: 25 November 2019 ·

Published Online: 17 December 2019



Partha Mukhopadhyay^{a)}  and Winston V. Schoenfeld^{a)} 

AFFILIATIONS

CREOL, The College of Optics and Photonics, University of Central Florida, Orlando, Florida 32816

^{a)}Electronic mail: partha.mukhopadhyay@creol.ucf.edu and winston@creol.ucf.edu

ABSTRACT

The authors report on high spectral responsivity ($\text{Sn}_x\text{Ga}_{1-x}$)₂O₃ Schottky UV photodetectors grown by plasma-assisted molecular beam epitaxy on β -Ga₂O₃ substrates. Schottky devices exhibited peak responsivities ranging from 49 to 194 A/W, with peak responsivity and wavelength position increasing systematically for higher Sn concentration from $x = 0.01$ to 0.18. Dark currents for the devices ranged from <1 nA to 3 μ A with rise and fall times in the 0.21–3 s time range, with slower response times likely due to photoconductive gain caused by trapped holes. Incorporation of up to 18% Sn into the tin gallium oxide (TGO) devices resulted in a redshift in the peak responsivity position, ranging from 5.19 to 4.86 eV, demonstrating tunability within the UV-C spectral region through Sn concentration adjustment. The authors believe this to be the highest reported responsivity for a planar Ga₂O₃-based Schottky photodetector to date, suggesting that TGO based UV-C Schottky detectors are an attractive approach toward deep-UV sensing applications.

Published under license by AVS. <https://doi.org/10.1116/1.5128911>

I. INTRODUCTION

Gallium oxide (Ga₂O₃) has received considerable attention from researchers in recent years due to its potential application in both electronic and optoelectronic devices. Of particular interest has been deep ultraviolet (UV) detectors that operate in the 100–280 nm UV-C spectral region. Prior work in more established compounds such as AlGa_N (Refs. 1–3) and MgZnO (Refs. 4–7) has realized some success, hindered primarily by materials' challenges. Though much less investigated to date, Ga₂O₃ compounds have already demonstrated considerable progress, with multiple groups demonstrating UV metal-semiconductor-metal (MSM)^{8–12} and Schottky^{13,14} detectors with performance that in many cases is competitive to that of AlGa_N and MgZnO.

While Ga₂O₃ epilayers have led to MSM and Schottky detectors that have strong UV photoresponse, prior work from our group has demonstrated that MSM devices based on ($\text{Sn}_x\text{Ga}_{1-x}$)₂O₃ [tin gallium oxide (TGO)] can outperform Ga₂O₃ devices, with the incorporation of a small concentration ($x < 0.1$) of tin into Ga₂O₃ increasing device response by more than one order of magnitude.¹⁵ Here, we present for the first time the impact of Sn incorporation into TGO on the performance of UV-C Schottky detectors based on TGO epilayers grown by molecular beam epitaxy (MBE) on native β -Ga₂O₃ substrates.

II. EXPERIMENT

Tin gallium oxide epilayers were grown by plasma-assisted MBE on (010) pieces of n -type ($n \sim 5 \times 10^{17} - 9 \times 10^{18} \text{ cm}^{-3}$) β -Ga₂O₃ substrates, sourced from Tamura (Japan). Oxygen was supplied by an SVT Associates plasma source, and standard Knudsen effusion cells were used to source Sn and Ga. Prior to growth, substrates were annealed at 780 °C for 30 min with an oxygen flow rate of 1.4 sccm and an RF power of 300 W to reduce surface contamination and improve structural surface quality. Epitaxial growth of the TGO epilayers was done at a substrate temperature of 600 °C with 2.5 sccm of oxygen at 300 W, resulting in a typical MBE chamber pressure of 1.7×10^{-5} Torr. Epitaxial growth was carried out for 3 h at a typical growth rate of ~80–90 nm/h, yielding an epilayer thickness of ~0.25 μ m. The epilayers were kept thin due to the short absorption length of UV-C radiation in Ga₂O₃ (Ref. 16) and sub-100 nm depletion width expected in the Schottky structure at low reverse biases. X-ray diffraction (XRD) on the epilayers was carried out a PANalytical X'Pert Cu- α_1 beam ($\lambda = 1.5405 \text{ \AA}$), and Sn composition in the films was determined using Rutherford Back-Scattering (RBS). Schottky devices were fabricated using standard photolithography methods. A Ti/Al/Ni (20/100/50 nm) Ohmic back contact was formed on the entire rear side of the n -type β -Ga₂O₃ substrate, annealed at 500 °C for 60 s in

nitrogen. Formation of the front side contact consisted of two primary steps accomplished with a standard lift-off procedure: (1) deposition of a high work function Pt ($\phi_m \sim 5.5$ eV) semitransparent layer (~ 3 nm) and (2) subsequent deposition of a thicker Ni/Au (20/130 nm) ring contact to aid in physical probing of the device. The thin Pt semitransparent contact enables deep-UV light transmission (estimated at $\sim 55\%$ at $\lambda = 245$ nm) from the top side of the device while still providing a suitable Schottky barrier, though we have not optimized its thickness to determine the best trade-off between transmission and Schottky performance. Two Schottky device sizes were fabricated, small and large, with a mesa diameter of 300 and 500 μm , respectively.

The current-voltage (I-V) and temporal characteristics of the Schottky photodetectors were measured with a Keithley 2400 source-meter SMU using probe tips to contact specific devices on the sample surface. Spectral responsivity was measured using a Newport CS260 UV-VIS monochromator fitted with a 30 W deuterium lamp. Light incident on the device was measured using a calibrated Si photodiode to enable absolute responsivity values to be determined. The spot size was roughly 4 mm^2 and was measured to have a power of 1.5 μW at 250 nm. When determining spectral responsivity for the devices, we measured incident power at each wavelength and factored in the area of the Schottky device in comparison to the spot size assuming uniform illumination.

III. RESULTS AND DISCUSSION

Figure 1(a) shows the XRD data for several samples with varying Sn concentration. The data contain clear peaks from the $\beta\text{-Ga}_2\text{O}_3$ substrate located at 54.5° , 60.5° , and 61° , corresponding to the (203), (-801), and (020) planes, respectively. Also observed is a broader peak located between 59° and 60° that is found to shift to lower angles and broaden with increasing Sn concentration. RBS

measurements of the epilayers grown with an Sn cell temperature of 660, 690, 750, and 780 $^\circ\text{C}$ indicated Sn concentrations of $<1\%$, 7%, 13%, and 18%, respectively, demonstrating a direct relation between the Sn cell temperature and percentage incorporation of Sn in the epilayers. For low Sn concentrations in the TGO alloy, we expect that the epilayer retains the monoclinic crystal structure of the underlying $\beta\text{-Ga}_2\text{O}_3$ substrate, though this requires further investigation since no such study of this alloy has been done to date. While transmission electron microscopy of the epilayer and the interface is required to verify the exact crystal structure, we do note that if it is indeed in the monoclinic arrangement this broader peak at 59° – 60° is likely the (113) TGO peak based on the Panalytical XRD database. The peak position of the (113) TGO peak as a function of Sn cell temperature is plotted in Fig. 1(b), demonstrating the systematic shift to lower angles with increasing Sn cell temperature (i.e., increasing Sn concentration from $<1\%$ to 18%). Based on the (113) peak position, we have calculated the lattice d-spacing for the epilayers in Fig. 1(b), showing a systematic increase for higher Sn concentrations.

TGO epilayers were fabricated into vertical Schottky devices. Figure 2 provides (a) a cross section of the basic device structure and (b) an optical photo of a full fabricated device showing the central circular Pt Schottky contact and top ring. Initial testing of the Schottky devices included measurement of the I-V characteristics with and without broad UV illumination directly from the 30 W deuterium light source (no monochromator). Figure 2(c) shows the typical I-V characteristics measured for the 300 μm (small) and 500 μm (large) TGO Schottky devices in the dark and with UV illumination from the deuterium lamp. The I-V characteristics follow the expected asymmetric behavior of a rectifying Schottky type device. The dark current was found to be in the nanoampere regime for most samples, offering an attractive noise floor that is competitive

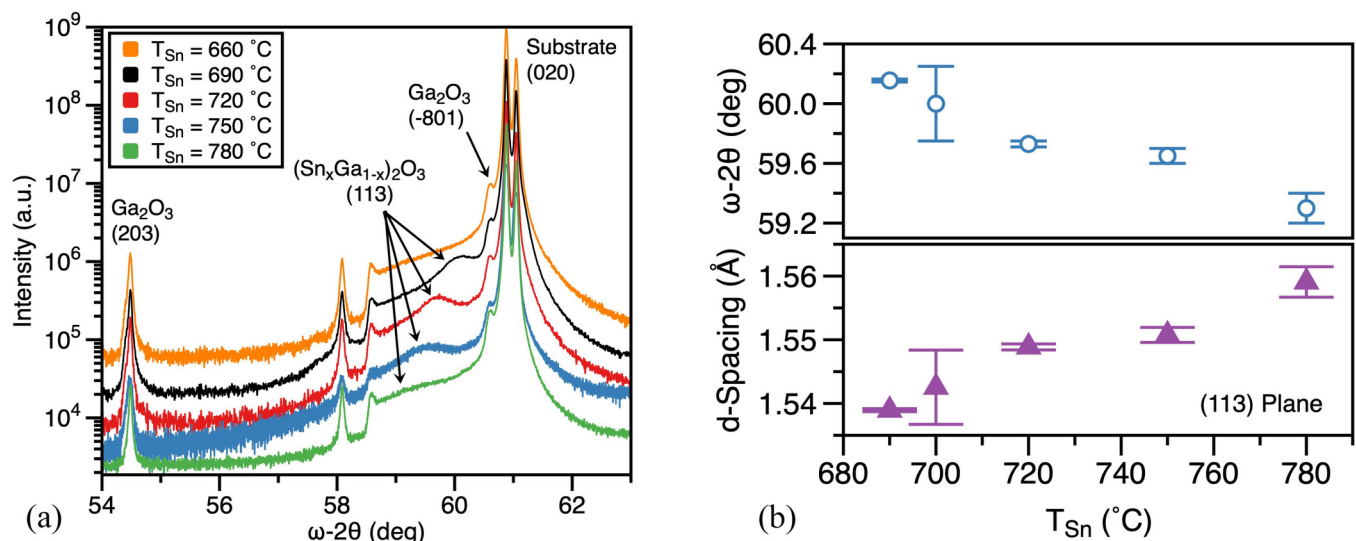


FIG. 1. XRD data (a) for TGO epilayers on n-type (010) Ga_2O_3 substrates and (b) observed shift and d-spacing of TGO (113) peak.

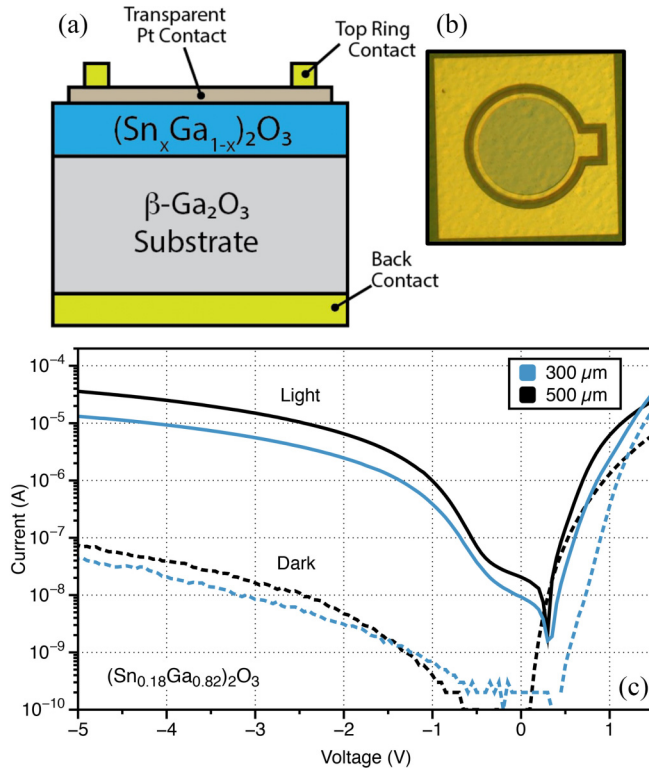


FIG. 2. TGO Schottky device cross section schematic (a), optical image of fabricated device (b), and typical I-V characteristics (c).

with other UV detectors. An exception was the lowest Sn concentration sample (<1% Sn) that was found to have a high dark current (microampere regime). We hypothesize that this may be due to Sn acting as a strong *n*-type dopant for low concentrations, making the epilayer very conductive in comparison to the TGO films with higher Sn concentrations. Table I provides a list of the dark currents measured for each sample. When illuminated with UV light, all devices show a strong increase in photocurrent that rises with increased reverse bias under constant UV illumination power [Fig. 2(c)]. While this initial test verifies strong UV photoresponse of the TGO Schottky devices, it does not verify the solar-blind properties.

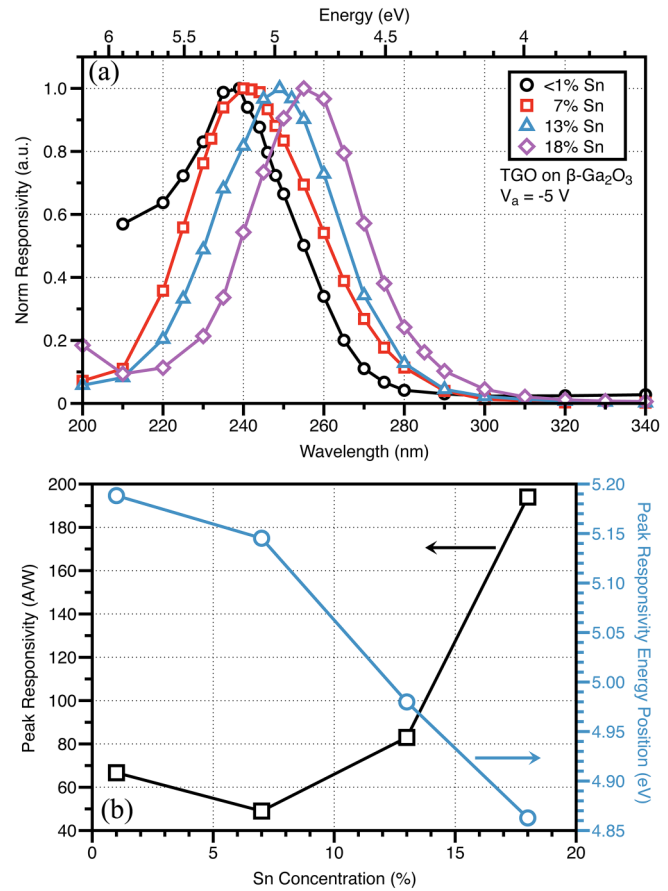


FIG. 3. Spectral responsivity (a) for various Sn concentration TGO Schottky detectors and (b) dependence of peak responsivity and peak response energy as a function of Sn concentration at $V_a = 5$ V.

To validate solar-blind functionality and determine the impact of Sn concentration on device properties, the spectral responsivity of the TGO detectors was measured for devices with Sn concentrations ranging from <1% to 18%. Figure 3(a) provides the measured spectral response of the different devices. We observe a clear red-shift in the peak response energy position as the Sn concentration increases, consistent with our prior work on TGO grown on

TABLE I. Summary of temporal characteristics and peak responsivity for TGO devices at $V_a = -5$ V.

Sn conc. (%)	Rise (s)		Fall (s)		Dark current	Peak respon. WL (λ_{peak}) (nm)	Rej. ratio (λ_{peak} : 340 nm)	Peak responsivity (A/W)
	τ_1	τ_2	τ_1	τ_2				
<1	0.97	16.62	0.21	8.06	3.1 μA	239	36:1	67
7	2.69	11.88	0.36	3.65	40.7 nA	240	394:1	49
13	2.89	17.44	0.34	14.12	0.329 nA	249	492:1	83
18	2.69	8.71	0.26	1.59	0.764 nA	255	169:1	194

sapphire.^{15,17} This is captured in Fig. 3(b) where we plot the peak response energy position (circular symbol) as a function of Sn concentration for the devices, showing a >300 meV redshift as Sn concentration increases from <1% to 18%. A redshift in the cutoff wavelength (10% peak responsivity) of the devices is also observed as Sn concentration is increased, demonstrating the ability to tune the spectral response of the Schottky detector through Sn concentration adjustment in the TGO. We also observe a measurable increase in absolute peak responsivity as the Sn concentration in the TGO is increased [see Fig. 3(b)]. For Sn concentrations of 7% and above, peak responsivity increases from 49 A/W to a value of 194 A/W for devices with 18% Sn. This is similar to what we have reported for lateral MSM TGO detectors on sapphire.^{15,17} For the <1% Sn sample, we observe a responsivity that is slightly higher than the next lowest Sn concentration device (7% Sn). This may be attributed to the high conductivity of the sample, as noted earlier, though we cannot fully explain this observation. Nevertheless, the trend of strong increases in the peak response of the devices for higher Sn concentrations is clear. The response ratios of the devices were determined by comparing the peak responsivity for the devices, located at the respective peak wavelength, λ_{peak} , to that at 340 nm. The values for λ_{peak} are provided in Table I along with the corresponding response ratios. We found typical λ_{peak} :340 nm response ratios to range from about 35 to 500.

Figure 4(a) provides the temporal characteristics of a 7% Sn TGO Schottky device. Such measurements were done for various TGO Schottky devices, and each was fitted with a double exponential to determine the τ_1 and τ_2 times for both the rise and fall segments. The basic equation used for fitting was

$$I(t) = I_0 + Ae^{-(t-t_0)/\tau_1} + Be^{-(t-t_0)/\tau_2}, \quad (1)$$

where A and B are scaling constants, t is the time, and τ_1 and τ_2 are the fast and slow decay constants, respectively. In all cases, the τ_1 times (both rise and fall) were found to be much faster than the τ_2 times. Figure 4(b) summarizes the τ_1 results obtained from fitting of the data of both the rising and falling edges. All τ_1 rise times were found to be in the second time range, with the 7%–18% TGO devices having slightly higher values than the <1% device. The τ_1 fall times of the devices were considerably faster, with all devices having values in the milliseconds regime. A full summary of τ_1 and τ_2 times is provided in Table I. In general, we do not see a clear systematic dependence of the rise/fall τ_1 values on Sn concentration, though we do note that the τ_1 rise times of the higher (7%–18%) Sn concentration TGO devices suggest these have a faster rise time than very low alloy concentration (<1%) TGO devices. We do observe considerable variation in the rise/fall τ_2 values of the TGO devices, but there does not appear to be any systematic trend with Sn concentration, suggesting that this is more dependent on the epitaxial film quality or fabrication process.

Despite the similarity of temporal characteristics, we find a significant variation in the peak responsivity of the TGO devices, with higher Sn concentrations leading to significant increases in the peak responsivity. As discussed earlier, this observation parallels our prior reported work on MSM TGO devices where higher

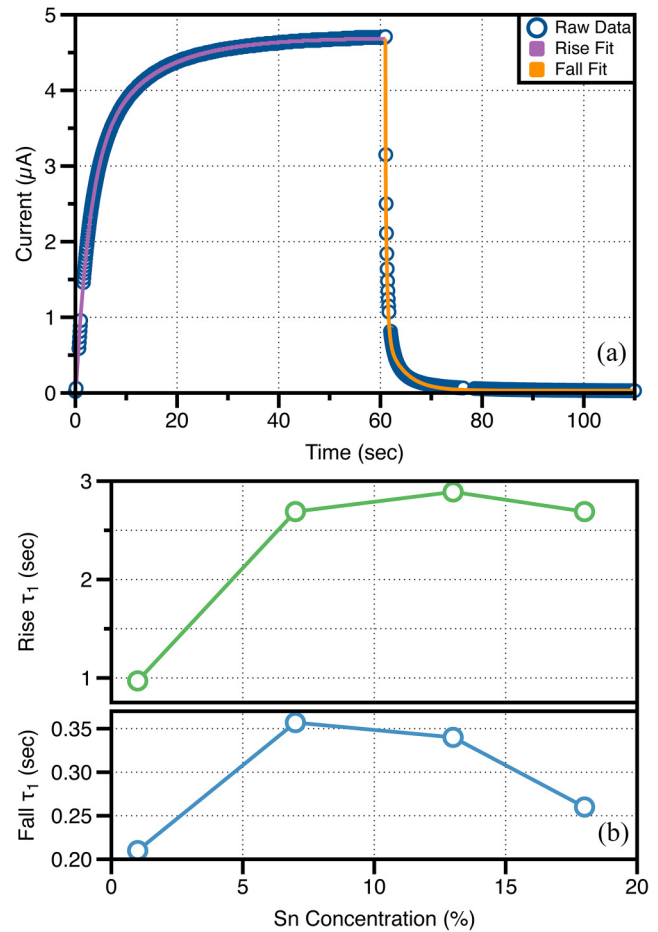


FIG. 4. Measured and fitted temporal data from 7% Sn TGO device (a) and rise/fall τ_1 times from fitting as a function of Sn concentration for devices.

Sn concentrations in TGO led to significant increases in peak responsivity.¹⁵

IV. SUMMARY AND CONCLUSIONS

In conclusion, we have demonstrated for the first time vertical TGO Schottky solar-blind detectors on β -Ga₂O₃ substrates. XRD suggests that TGO epilayers retain the monoclinic phase of the β -Ga₂O₃ substrate, with a broad peak at $\sim 60^\circ$ in the ω -2 θ scan that shifts to lower angles with increasing Sn concentration, though more investigation is required to verify the exact behavior. Solar-blind vertical Schottky devices demonstrated strong rectifying behavior with dark currents in the nanoampere regime. The energy position of the peak responsivity was found to systematically redshift by >300 meV for increasing Sn concentrations from <1% to 18% in the TGO epilayers. As we have reported for MSM TGO devices, peak responsivity increased for higher Sn concentrations, ranging from 49 to 194 A/W over the composition range

investigated. Temporal measurements indicated rise and fall times in the second and millisecond time regimes, respectively, with no strong systematic trend with Sn concentration. This work demonstrates the viability of solar-blind TGO based vertical Schottky detectors, with tunable cutoff and peak responsivity wavelengths through Sn concentration adjustment, that offer improved responsivity over Ga₂O₃ counterparts.

ACKNOWLEDGMENT

The authors would like to acknowledge support from the Army Research Office under Project Award No. W911NF-17-1-0377, monitored by Michael Gerhold.

REFERENCES

- ¹S. V. Averine, P. I. Kuznetsov, V. A. Zhitov, and N. V. Alkeev, *Solid State Electron.* **52**, 618 (2008).
- ²M. Gökkavas, S. Butun, T. Tut, N. Biyikli, and E. Ozbay, *Photonics Nanostructures: Fundam. Appl.* **5**, 53 (2007).
- ³E. Ozbay, N. Biyikli, I. Kimukin, T. Kartaloglu, T. Tut, and O. Aytur, *IEEE J. Sel. Top. Quantum Electron.* **10**, 742 (2004).
- ⁴M. Toporkov, P. Mukhopadhyay, H. Ali, V. Beletsky, F. Alema, A. Osinsky and W. V. Schoenfeld, *Proc. SPIE* **10105**, 101051N (2017).
- ⁵F. Alema, O. Ledyayev, R. Miller, V. Beletsky, B. Hertog, A. Osinsky and W. V. Schoenfeld, *Proc. SPIE* **9749**, 97490Y (2016).
- ⁶F. Alema, B. Hertog, O. Ledyayev, D. Volovik, R. Miller, A. Osinsky, S. Bakhshi, and W. V. Schoenfeld, *Sens. Actuators A Phys.* **249**, 263 (2016).
- ⁷W. V. Schoenfeld, M. Wei, R. C. Boutwell and H. Liu, *Proc. SPIE* **8987**, 89871P (2014).
- ⁸L. X. Qian, Y. Wang, Z. H. Wu, T. Sheng, and X. Z. Liu, *Vacuum* **140**, 106 (2017).
- ⁹F. Alema *et al.*, *Phys. Status Solidi A* **214**, 1770127 (2017).
- ¹⁰Q. Feng *et al.*, *IEEE Trans. Electron Devices* **63**, 3578 (2016).
- ¹¹Y. Guo, Z. P. Wu, Y. H. An, X. C. Guo, X. L. Chu, C. L. Sun, L. H. Li, P. G. Li, and W. H. Tang, *Appl. Phys. Lett.* **105**, 023507 (2014).
- ¹²T. Oshima, T. Okuno, and S. Fujita, *Jpn. J. Appl. Phys.* **46**, 7217 (2007).
- ¹³E. Farzana, Z. Zhang, P. K. Paul, A. R. Arehart, and S. A. Ringel, *Appl. Phys. Lett.* **110**, 202102 (2017).
- ¹⁴F. Alema, B. Hertog, A. Osinsky, P. Mukhopadhyay, M. Toporkov, W. V. Schoenfeld, E. Ahmadi, and J. Speck, *Proc. SPIE* **10105**, 101051M (2017).
- ¹⁵P. Mukhopadhyay and W. V. Schoenfeld, *Appl. Opt.* **58**, D22 (2019).
- ¹⁶M. F. Al-Kuhaili, S. M. A. Durrani, and E. E. Khawaja, *Appl. Phys. Lett.* **83**, 4533 (2003).
- ¹⁷P. Mukhopadhyay, M. Toporkov, and W. V. Schoenfeld, *Proc. SPIE* **10533**, 105330V (2018).